

## MICROSTRUCTURE, MICROHARDNESS AND CHEMICAL COMPOSITION OF A DETAIL OBTAINED BY ELECTRO-ARC SURFACING ON A HARDWARE-SOFTWARE COMPLEX OF A DELTA LAYOUT

## MIKROSTRUKTURA, MIKROTVRDOĆA I HEMIJSKI SASTAV DELA SKLOPA U IZVOĐENJU ELEKTROLUČNIM NAVARIVANJEM NA HARDVER-SOFTVER KOMPLEKSU TIPRA DELTA


Originalni naučni rad / Original scientific paper



Rad primljen / Paper received: 3.02.2023

<https://doi.org/10.69644/ivk-2024-03-0351>

Adresa autora / Author's address:

<sup>1)</sup> National Research Tomsk Polytechnic University, Tomsk,

Russian Federation M.A. Kuznetsov  0000-0003-3919-3009;

A.V. Proskokov  0000-0003-3526-4674; D.P. Il'yaschenko  0000-0003-0409-8386 \*email: [mita8@rambler.ru](mailto:mita8@rambler.ru)

<sup>2)</sup> Institute of Strength Physics and Materials Science of Siberian Branch Russian Academy of Sciences, Tomsk, Russian Federation

<sup>3)</sup> Pryazovskyi State Technical University, Mariupol, Russian Federation E.V. Lavrova  0000-0001-6030-0986

### Keywords

- electric arc surfacing with metal wire
- microstructure
- microhardness
- chemical composition

### Abstract

*In the work, electric arc layer-by-layer surfacing of a low-carbon low-alloyed wire in a carbon dioxide environment is carried out. The deposited metal structure in the form of a parallelepiped of thickness 4 mm and height 40 mm reveals the study of microstructure by optical microscopy, the composition of microhardness by indentation of drop tips and chemical composition by atomic emission spectral analysis. The obtained results show that products have a gradient structure. Only the last deposited zone has a dendritic structure. The underlying zones of secondary heat treatment, due to heat release from the upper layer, have a polyhedral recrystallized fine-grained ferritic-pearlitic structure. The microhardness of ejected deposited fibres changes from 1760 MPa to 1360 MPa in upper deposited layers. This is a general decrease in the pearlite fraction and the definition of ferrite. The evaluation of the chemical composition of deposited metal shows that in the first-fourth case, the metal of the deposited wire and substrate metal change, and the percentage of chemical elements in the thickness with the sixth composition of twenty approximately determines the metal of the deposited wire.*

### INTRODUCTION

Currently, one of the most promising areas for implementing technological processes for manufacturing metal products of complex configuration is additive manufacturing. It is based on layer-by-layer metal surfacing in accordance with a three-dimensional model created by computer modelling and design, /1/. Metal powders of the micron range /2-17, 48/, or wire of the required diameter /11-68/ of various chemical compositions are used as the starting material. An electronic /2, 3, 5-11, 17-19, 29-31, 53/, laser /2-5, 7-19, 23-28, 53/, or plasma beam is used as an energy (heat) source, and also an electric arc /15-17, 32-67, 69, 70/. In addition, it is possible to use hybrid heat sources, e.g., a combined electric arc and laser beam, /61/.

### Ključne reči

- elektrolučno navarivanje metalnom žicom
- mikrostruktura
- mikrotvrdoća
- hemijski sastav

### Izvod

*U radu se izvodi elektrolučno navarivanje sloj-po-sloj niskougličeničnom niskolegiranim žicom u zaštiti ugljen-dioksidom. Naneta struktura metala, oblika paralelopipeda debljine 4 mm i visine 40 mm, je poslužila za određivanje mikrostrukture optičkom mikroskopijom, sastava mikrotvrdoćom utiskivanjem i hemijskog sastava metodom spektralne analize emisije atoma. Dobijeni rezultati pokazuju da dobijeni proizvodi imaju gradijentnu strukturu. Samo je poslednji sloj imao dendritnu strukturu. Prethodni slojevi, dvostruko termički obrađeni, usled oslobađanja toplote gornjeg sloja, imaju poliedarsku rekristalizovanu fino-zrnu feritno-perlitnu strukturu. Mikrotvrdoća izbačenih nanetih vlakana se menja od 1760 MPa do 1360 MPa u gornjim nanetim slojevima. Ovo je istovremeno i opšti pad frakcije perlita i po definiciji ferit. Određivanje hemijskog sastava nanetog metala pokazuje da u prvom-četvrtom slučaju, dolazi do promena u metalu navarene žice i u metalu supstrata, kao i u procentu hemijskih elemenata po debljini sa šestim sastavom od dvadeset približno uslovljava metal žice za navarivanje.*

Among the listed methods for manufacturing metal products by additive technologies, one of the most optimal is layer-by-layer surfacing of wires. This is due to several reasons. Firstly, there is a wide range of chemical composition and diameter of wires on the market that can be used as a material for electric arc surfacing. Secondly, the nomenclature of production complexes for this process is open. This allows the use of both industrial robots and automated three-axis tables in conjunction with common power sources, torches and ancillary equipment designed for conventional arc welding and surfacing. These factors, together with the relatively high productivity of arc surfacing, make these technologies promising despite the surface quality of manufactured products and the need for their subsequent machining, as well as residual deformations and stresses.

However, the implementation of layer-by-layer surfacing process is hampered by the fact that the cost of specialised equipment and software does not correlate with the possibility of its use by industrial machine-building enterprises. Attempts to implement layer-by-layer surfacing technology are reduced to the use of CAM modules that generate a control programme for CNC milling machines or plasma cutting machines. The main disadvantage of using such software modules is a significant difference in the specifics of the ongoing processes. So, in contrast to machining with a multi-blade tool, where the tool parameters are taken into account in the trajectory of the executing body, in the process of layer-by-layer deposition of the part wall, it is necessary to ensure the uniformity of metal deposition, taking into account the temperature and speed parameters for supplying the required volume of molten metal. Compared with the possibility of plasma cutting machines, the trajectory formed for cutting the material completely repeats the contour of the cut part, and for surfacing a wall whose thickness is greater than the geometric parameters of the weld pool, it is necessary to use complex motion elements to fully ensure the geometry of the created part. In addition, in the layer-by-layer surfacing process, it is necessary to take into account the parameters of the accumulating medium, which will change depending on the shape and size of the obtained surfaces of the part and change the physical and mechanical characteristics after the metal cools down.

Therefore, the issue of developing a software and hardware complex for the manufacture of complex body parts by layer-by-layer surfacing becomes relevant. This software package will allow you to move the burner along a complex predetermined trajectory and obtain a wall of the deposited product of required thickness and configuration, and this will ensure uniform physical and mechanical properties of the material throughout the entire volume of the part. The main difference of this work is that the developed software package is adapted to layer-by-layer metal surfacing from all-metal welding wire and is synchronized with the electronic-mechanical complex for layer-by-layer arc surfacing in shielding gases. The significance of the obtained results lies in the fact that they will make it possible to manufacture unique products without traditional methods for producing metal blanks by casting in conditions of single production and, at the same time, significantly reduce the number of surface machining operations in the technological process of manufacturing metal products.

In order to test the hypothesis on the possibility of implementing the surfacing process in automatic mode along a given trajectory, the authors designed a three-coordinate system for moving the welding torch holder. The installation is based on the 'Cartesian kinematics' system with perpendicularly located guiding elements and traction devices of the screw-nut type. The burner is installed vertically, and its upward movement corresponds to the Z coordinate. The rectangular table is able to move in the horizontal plane in the X and Y coordinates, respectively.

The stepper drives are controlled by an eight-bit Arduino UNO R3 ATmega 328P microcontroller with free distributed GRBL firmware installed. To implement the movement

according to the programme, an appropriate language based on G and M commands is used. In the process of testing the designed installation, its serious shortcomings are revealed. For example, when growing a part in layers, it is necessary to move the table in a horizontal plane while the table mass increases which means that the inertial component becomes larger. Also, in the process of working out using a conventional G code, when changing the direction of movement, the GRBL module creates an acceleration and deceleration of movement speed which leads to instability in welding arc formation. An important negative factor are open areas of mechanical and electrical installation parts, when molten metal drops hit them. However, despite the existing shortcomings, it is possible to obtain several completed samples obtained by welding wire surfacing. The authors have outlined ways to improve both mechanical performance and software process improvement.

The purpose of this work is to develop a software and hardware complex for the production of hull products with different wall thicknesses and different configurations by layer-by-layer metal deposition from all-metal welding wire in a shielding gas environment. The bulk of the specialised equipment and software present on the market does not correlate with the possibility of its use by industrial machine-building enterprises due to the high price. The developed software and hardware complex is in this case a very good alternative, since it is much cheaper than analogues and has high performance.

#### PRESENTATION OF THE MAIN MATERIAL

To develop a hardware-software complex, the design, modelling, and programming methods are applied.

When designing a software and hardware complex, it is important to take into account the workspace in which work will take place, technological, kinematic capabilities and features of the tasks it must perform. To determine the working area dimensions of the hardware-software complex and the dimensions of the resulting product, it is necessary to find dependences of geometric parameters of the complex on the trajectory of the output link. Also, one of the most important stages in the design of a robotic mechanical system is the solution of the problem of structural synthesis of mechanisms. An inefficient mechanism design from a structural point of view will lead to excessive loads on kinematic pairs, /71, 72/.

In the process of modelling the design of the software and hardware complex, one of the main conditions is that all mechanical and electrical parts are not in the surfacing zone, because of splashing, present during welding with a consumable electrode in a shielding gas environment, that can disable them. The next condition is to ensure movement of the welding torch itself, by analogy with a robotic arm, and not a table, as in metal-cutting equipment. Note that with each deposited layer of metal, the weight of the part increases, which means that loads on the mechanisms also increase. The third condition is to ensure the resistance of the structure to high temperatures in the welding wire melting process. In the process of arc layer-by-layer surfacing, heat is released, and the structure may be heated, which can lead to deformation of main components.

The general composition of the complex should include such basic parts as a perfect kinematic design for moving the welding torch, an electronic component that includes a fast microcontroller and software for preparing control programmes that form a trajectory, taking into account physical and technological processes and geometric shapes (Fig. 1).

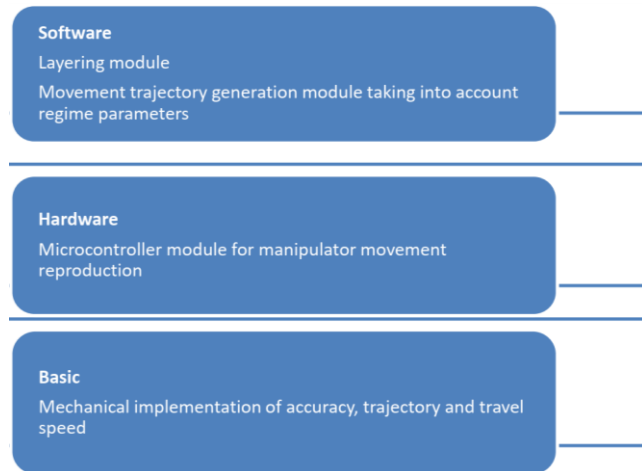


Figure 1. General composition of the software and hardware complex for surfacing with welding wire.

The new software and hardware complex mechanism is based on the operation of a manipulator with parallel kinematics 'delta' layout. This manipulator consists of an upper fixed round base with a radius  $R$  (Fig. 2) and a lower moveable platform with a smaller radius  $r$  (Fig. 2). The platforms are connected by three levers. Each lever is divided into two parts: the upper arm of length  $l_1$  (Fig. 2) is fixed to the motor with one end on the upper base and rotates through an angle  $\theta$ , the lower arm of length  $l_2$  (Fig. 2) consists of two parallel-connected rods that can freely rotate on the hinge - spherical connection. Each double arm is connected to the upper arm also through a spherical joint in such a way that its upper side always remains perpendicular to its arm and parallel to the plane of the upper base. The combination of

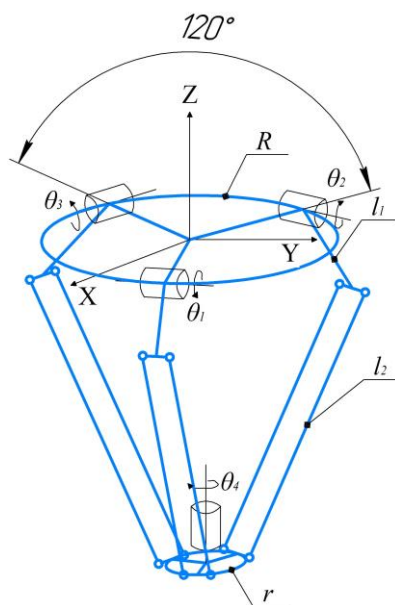


Figure 2. Scheme of a manipulator with lever-parallel kinematics.

degrees of freedom of the hinge allows the lower moveable platform of the manipulator to always remain parallel to the upper base, where the welding torch will be placed.

The position of the lower platform determines the angle of rotation of the upper arms by rotating Nema 23 stepper drives with precise planetary gears.

To calculate the position of the moving part of the manipulator, it is necessary to compare the angles of rotation of the lever with required Cartesian coordinates in the XYZ system. In other words, it is necessary to solve the inverse problem of kinematics. In the second task, the angles of the levers  $\theta_1$ ,  $\theta_2$ , and  $\theta_3$  are known (Fig. 2) and it is necessary to find the current XYZ position of the welding torch in order to move it to a given distance. This is a direct kinematic problem.

The design of the delta manipulator implies that each lever can rotate only in one plane, while describing a circle with radius, if centred at the point of fixation to the engine. The lower arms use spherical joints, and each arm is free to rotate around a sphere centred on the attachment point to the lower platform. Therefore, the coordinates of the platform and the angle of rotation of the lever are easily calculated from the laws of trigonometry and the intersection of spherical coordinates.

Taking into account the need for a large amount of mathematical transformations to ensure the synchronism of movement of each rotation drive, the project uses a microcontroller based on a 32-bit LPC1768 processor. That has provided smooth running and high speed with accelerated movements of the manipulator.

A three-dimensional model prepared in stl format was divided into sections using 3D printing software with plastic, and for each section a programme contour is prepared using linear interpolation with a minimum step even in radius sections. This subsequently made it possible to ensure the uniformity of movement of the burner in curved sections.

According to the above conditions, a software and hardware complex is developed and manufactured, which makes it possible to manufacture complex body parts with various configurations and wall thicknesses by layer-by-layer surfacing of a metal wire in a shielding gas environment.

In this work, a welding wire of diameter 0.8 mm of the following chemical composition is used as deposited material: carbon 0.05-0.11 %, silicon 0.7-0.95 %, manganese 1.8-2.1 %, nickel up to 0.25 %, chromium up to 0.2 %, nitrogen up to 0.01 %, sulphur up to 0.025 %, phosphorus up to 0.03 %. Surfacing took place on a substrate with a size of 50×50×5 mm of the following chemical composition: carbon 0.38-0.49 %, silicon 0.15-0.3 %, manganese 0.5-0.8 %, nickel up to 0.3 %, chromium up to 0.3 %, copper up to 0.3 %, nitrogen up to 0.008 %, sulphur up to 0.025 %, phosphorus up to 0.03 %. Surfacing was carried out using a FUBAG IRMIG 200 SYN power source. Products were formed in the following modes: current strength 70-80 A, voltage 18-20 V, deposition rate 100 mm/min. All these parameters are chosen depending on the configuration and wall thickness of the deposited product. Carbon dioxide is used as a protective gas. The creation of a computer 3D model took place in the Compass-3D software systems.

To study the microstructure, the sample was divided into four zones of equal size (Fig. 3). Next, templates 2.5 mm thick were made. The templates were cut according to the scheme shown in Fig. 3 by electric spark cutting on a Delta-Test Arta 151 machine.

Thin sections were made on the templates. In the manufacture of sections, mechanical grinding, mechanical polishing with ASM 10/7 NVL diamond paste, and chemical etching in a 4 % alcoholic solution of nitric acid were used. The structure was studied by optical metallography on a Neophot-21 microscope with images recorded using a Genius VileCam digital camera. Microhardness was determined on a microhardness tester (diamond tips indentation) in zones shown in Fig. 3. The load on the indenter is 1 N (100 g). The number of measurements per point is three. The assessment of the chemical composition was carried out in zones shown in Fig. 3 by method of atomic emission spectral analysis using an optical emission spectrometer DFS - 500.

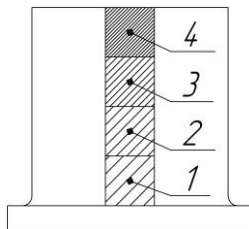


Figure 3. Sample preparation scheme for structure studies.

The developed software and hardware complex (Fig. 4) includes two main components:

- algorithms and a computer programme for calculating a complex trajectory of movement of the executing body and generating a control programme for a three-coordinate CNC system designed for layer-by-layer surfacing of metal wire, taking into account the geometric parameters of the product;
- an electronic-mechanical complex equipped with a CNC system that allows torch movement along a given complex

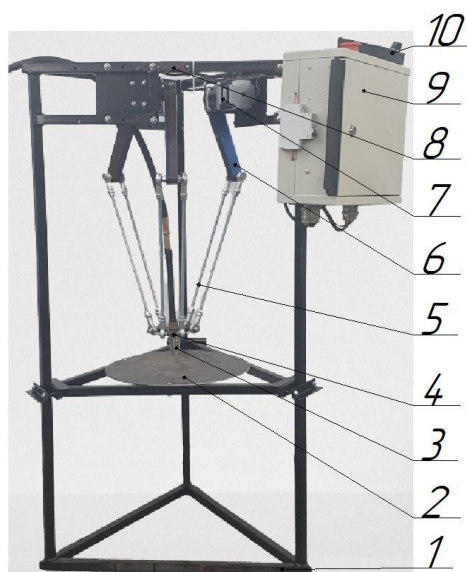


Figure 4. Hardware and software system: 1-frame, 2-table, 3-welding torch, 4-welding torch holder, 5-guide, 6-lever, 7-stepper motor with gearbox, 8-limit switch, 9-control unit, 10-touch screen.

trajectory and obtains a wall of the deposited product of the required thickness and configuration by melting an all-metal welding wire in a shielding gas environment.

Development of modes for multilayer metal surfacing with the help of developed software and hardware complex consists in conducting experimental studies of the process of formation of deposited layers in a shielding gas environment with a consumable electrode. The developed mathematical model makes it possible to establish operating ranges of modes and identify the best ratios of parameters for the formation of stable high-quality layers of the resulting part. Accumulated data will form the basis of the regime features of the software and hardware complex.

Formation of a complex torch trajectory consists in filling the deposited layer using a given strategy for filling the volume with molten metal. Initial data for the formation of the trajectory is wall thickness  $b$  (Fig. 5), the step of forming trajectory element  $h$  (Fig. 5), angle of deviation from rectilinear motion, radius  $r$  (Fig. 5). Parameters  $h$  and  $r$  depend on the parameter  $b$ . The results obtained during the work on the software module make it possible to use algorithms for the formation of a complex multilayer torch trajectory for layer-by-layer surfacing of the walls of body parts with a welding wire. To obtain a product with a wall thickness of up to 5 mm, a rectilinear welding torch movement is sufficient. For wall thicknesses greater than 5 mm, one of the filling strategies shown in Fig. 5 must be used.

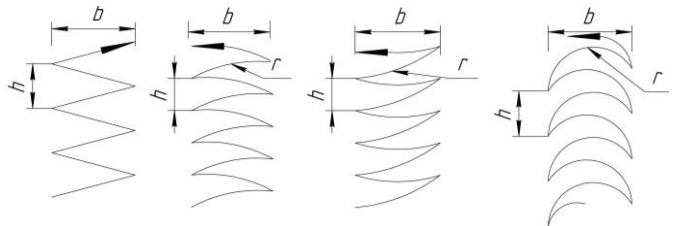


Figure 5. Metal volume filling strategy options.

A series of experiments was carried out using the manufactured software and hardware complex and a mathematical model was compiled that describes dependences of input, output, and variable parameters, such as: current strength, voltage, surfacing speed, wire feed speed, taking into account the chosen strategy for filling the thickness of the deposited wall. Based on the statistical processing of research results, an objective function is obtained in the form of an equation in which optimisation criteria are determined from the point of view of qualitative characteristics of the obtained surfaces. The data obtained on the basis of the mathematical model are used for algorithms in the formation of torch trajectory during surfacing, which ultimately will make it possible to obtain body products by method of layer-by-layer metal surfacing from all-metal welding wire with required wall thickness.

Using the software module, the modes for layer-by-layer surfacing (current, voltage, surfacing speed, wire feed speed, etc.) and torch movement modes (travel step, movement trajectory, movement speed, etc.) are calculated depending on the required thickness and geometric configuration of the body part wall.

Work on the software and hardware complex can be divided into several main stages:

1- Creation of a computer 3D model of the manufactured product using CAD systems (Fig. 6). Parallelepiped with a wall thickness of 4 mm.

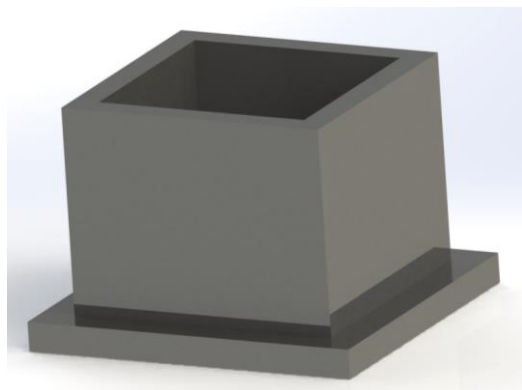


Figure 6. 3D sample model.

After construction, the model is divided into layers depending on the required value of the deposited layer (Fig. 7). In this case, 20 layers 4 mm wide, 2 mm high.

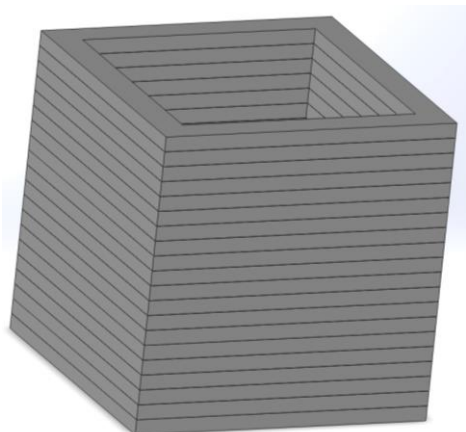


Figure 7. Displaying layers on 3D models.

When building a model, the wall thickness is taken with an allowance of 1-2 mm for subsequent machining of the product.

2- The creation of a G-code for one section is implemented using specialized Planet CNC software. One section of the product is saved in dxf format. The dxf file is opened in the CNC USB Controller programme to generate the G-code. The G-code includes all necessary data for surfacing a metal product according to the developed model: the origin of coordinates (the point at which surfacing begins). It is possible to programme several options for surfacing: (all layers begin to grow from the same place (Fig. 8a), in this case it is necessary to take into account that at the end of the surfacing of the layer, the welding arc must still burn for 1-2 s in order to avoid formation of a crater during the attenuation of the welding arc; each layer begins to build up with an offset from the start of welding of the previous layer by 2-3 mm (Fig. 8b); each layer starts to build up from a programmed point (Fig. 8c) /73/. The second and third options are the most optimal for electric arc surfacing, because they allow to avoid formation of a crater during the attenuation of the welding arc and increase the cooling time of the product between deposited layers), the step, speed and trajec-

tory of the torch, the amount of a single torch rise after each deposited layer, the number of layers. All these parameters are set depending on the configuration and wall thickness of the deposited product. The file with the G-code is saved in a text format and then opened in specialized Grbl Controller software for surfacing.

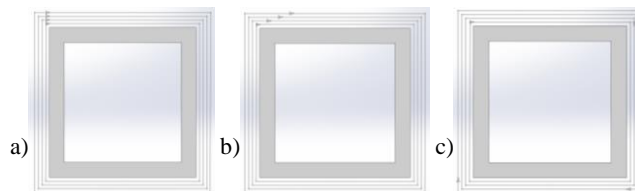


Figure 8. Scheme of the trajectory of layer surfacing (arrows show the beginning of surfacing of each layer).

3- Layer-by-layer formation of products occurs on the substrate. The substrate is placed on a fixed table. The welding torch, which provides precise positioning and movement along X, Y, Z coordinates, is set using Grbl Controller software to the zero point (the point at which surfacing begins). The distance from end of electrode wire to substrate is 6 mm. Torch movement speed is in X, Y coordinates. The movement speed and amount of one-time movement of the welding torch in Z coordinate is set using CNC USB Controller software. The 'start' button is pressed, the welding wire starts to feed, and the welding torch moves at a given speed in accordance with the programme, the welding arc ignites. The substrate begins to melt, forming a liquid molten mass of shallow depth. The wire is fed at a predetermined speed into the melting zone and partially melts, forming a layer. After the first layer is deposited, the welding arc goes out, the torch moves along the Z coordinate by 3 mm and to the next programmed point along XY coordinates, the process is repeated. After all layers have been deposited, the welding torch stops, and the welding arc goes out. In this work, surfacing is carried out along the trajectory shown in Fig. 8c. The height and width of the layer depends on the speed of the welding torch, deposition modes, and the diameter of the welding wire. The image of the product obtained by this method is shown in Fig. 9.



Figure 9. Metal structure in the form of a parallelepiped with wall thickness of 4 mm and height of 40 mm.

4- Calculation of modes for layer-by-layer surfacing (current, voltage, surfacing speed, wire feed speed). These parameters are calculated depending on the configuration and wall thickness of the deposited product. Properly selected surfacing modes will ensure uniform physical and mechanical properties of the material throughout the entire volume of the part.

5- Machining of a metal product occurs depending on the requirements for the product.

Microstructural studies are carried out on a product consisting of twenty layers. The scheme of sample preparation for the study of the structure is shown in Fig. 3.

Analysis of the results of metallography show that each of the deposited layers has a structure with different grain size and morphology.

Zone 4, deposited last and directly adjoining the free surface, has a cast metal structure consisting of misoriented strongly branching dendrites (Fig. 10). Influence of welding direction has no effect on the orientation of dendrites.

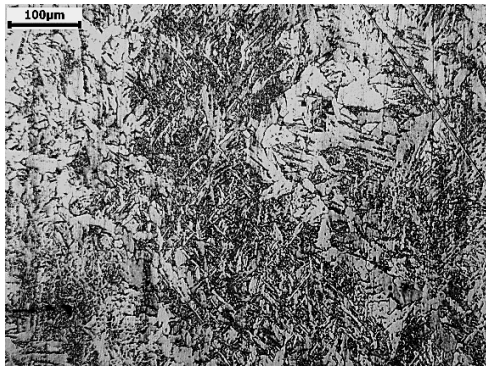


Figure 10. Zone 4 structure.

Figure 11 shows that all previously deposited zones 3, 2, 1 have a polyhedral recrystallized fine-grained ferrite-pearlite structure. In zone 3 (Fig. 11a), the size of ferrite grain corresponds to grain grade 9 and is  $16.4 \pm 8.7 \mu\text{m}$ . Pearlite content corresponds to the chemical composition of deposited wire. In the underlying zone 2 (Fig. 11b), where recrystallization occurs twice, the size of the ferrite grain corresponds to a grain score of 10 and is  $12.7 \pm 6.6 \mu\text{m}$ . In terms of phase composition, the structure also corresponds to the deposited wire. The grain is even finer in zone 1 (Fig. 11c), where there was a partial mixing of molten metal of the deposited wire and substrate metal. Therefore, in zone 1, the pearlite content is higher than in weld metal, but less than it should be in the base metal. In this layer, the size of ferrite grain corresponds to grain grade 11 and is  $7.3 \pm 3.7 \mu\text{m}$ .

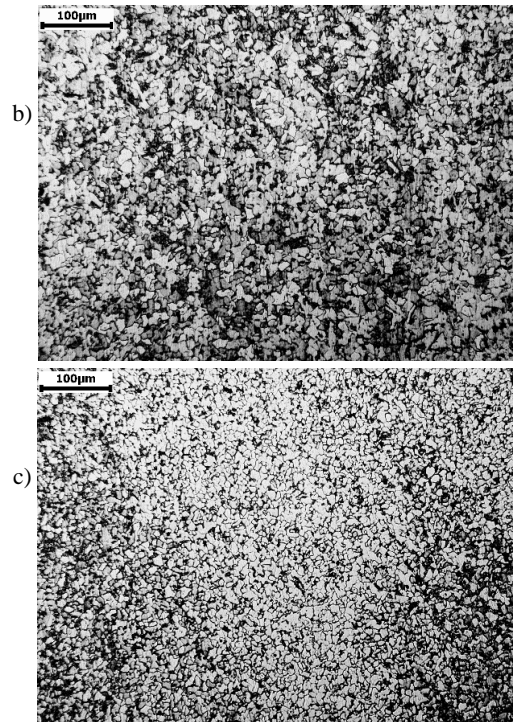
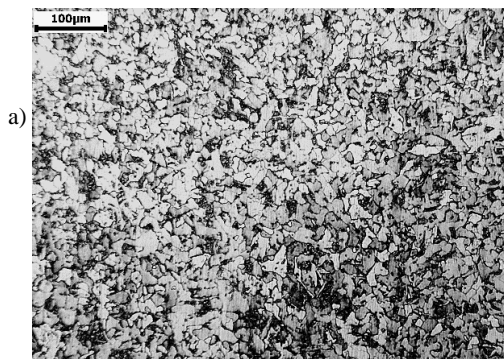


Figure 11. Structure of deposited metal in layers subjected to recrystallization: a) zone 3; b) zone 2; c) zone 1.

Thus, the deposited metal has a gradient structure with an exponentially increasing grain size as it moves away from the substrate. The gradient structure is due to the change in heat removal conditions as the surfacing progresses. Near the free surface (zone 4), heat removal is less; therefore, crystallization proceeds according to the mechanism of formation of relatively short, highly branched and non-dominantly oriented dendrites. In the rest of the deposited metal, a typical polyhedral recrystallized fine-grained ferrite-pearlite structure occurs. According to generally accepted concepts [74], the less the dendritic structure is manifested and the less coarse the dendrite structure is, the better are the mechanical properties of the deposited metal. Due to the fact that there is a change in phase composition by a decrease in pearlite component in the structure and an increase in the ferrite component from zone 1 to zone 4, a regular decrease in microhardness is observed (Fig. 12).

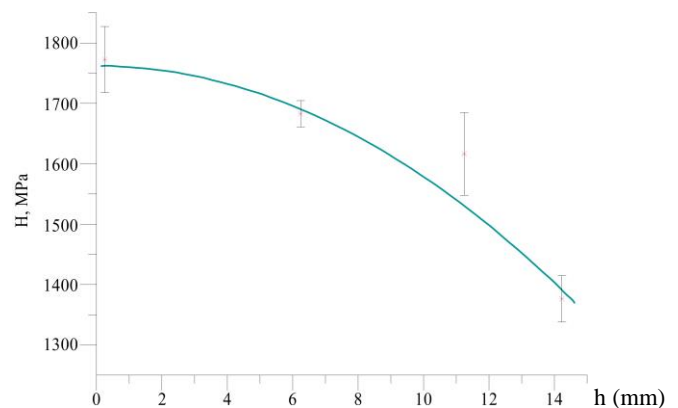


Figure 12. Layer-by-layer change of microhardness in surfacing; points on the graph correspond to zones 1-4.

These data do not contradict the assessment of the chemical composition of the deposited metal. The obtained results are shown in Fig. 13. In zone 1, the metal of the deposited wire and substrate metal are mixed, and the percentage of chemical elements in zones 2, 3, and 4 is almost identical to the metal of the deposited wire.

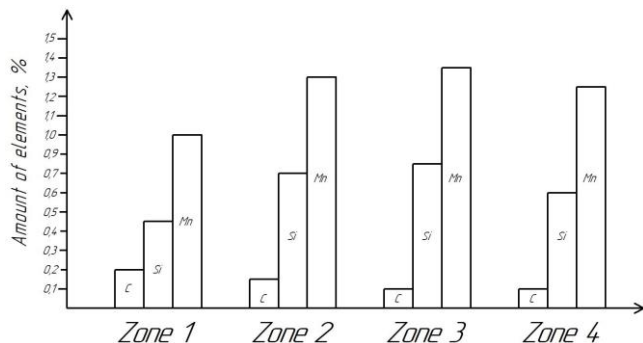


Figure 13. Chemical composition of elements in zones 1-4.

Increasing the percentage of manganese and silicon in the weld body (weld metal: Mn 0.5-1.35 %, Si 0.25-0.75 %) relative to the base metal (base metal: Mn 0.5-0.8 %, Si 0.15-0.3 %) is due to the fact that these elements are transferred from the weld metal (surfacing metal: Mn 1.8-2.1 %, Si 0.7-0.95 %). The presence of manganese in the deposited wire helps to reduce the burnout of silicon and, conversely, the presence of silicon in the weld wire helps to reduce the burnout of manganese. The higher the content of silicon and manganese in the deposited wire, the lower their burnout. Despite the lower chemical affinity for oxygen, manganese burns out more than silicon, /75/.

This confirms that the percentage ratio of chemical elements in the weld metal is almost identical to the metal of the deposited wire. The increased percentage of carbon in zone 1 (C 0.2 %) compared to the weld metal (weld metal: C 0.05-0.11 %) is due to the fact that it passes into the weld pool from the substrate metal. The decrease in percentage of carbon in zone 2 (C 0.15 %) compared to zone 1 (C 0.2 %) indicates that there is no transfer of carbon from the substrate metal. The percentage of carbon in zones 3-4 (C 0.1 %) corresponds to the percentage of carbon in the weld metal (weld metal: C 0.05-0.11 %). This is due to the fact that there is no carbon burnout due to low welding mode parameters (current 70-80 A, voltage 18-20 V). Chrome and nickel are also present in the deposited metal, but their percentage ratio is minimal up to 0.1 %.

## CONCLUSIONS

Designed, developed and manufactured hardware-software complex delta layout allows to obtain metal products of complex shape in automatic mode by means of electric arc layer-by-layer surfacing due to melting of the welding wire.

It has been determined that in the case of arc layer-by-layer surfacing, the walls of products have a gradient structure. Only the last deposited layer has a dendritic structure. The underlying layers are subjected to secondary heat treatment due to the heat release of the upper layer.

The decrease in microhardness from zone 1 to zone 4 is due to a decrease in the ratio of the pearlite component in the structure and an increase in the ferrite component.

The increase in the percentage ratio of manganese and silicon in the deposited product relative to the substrate metal is due to the fact that these elements are transferred from the deposited metal. The increased percentage of carbon in zone 1 compared to the deposited metal is due to the fact that it passes into the weld pool from the substrate metal. The decrease in percentage of carbon in zone 2 compared to zone 1 (C 0.2 %) indicates that there is no transfer of carbon from the substrate metal. The percentage of carbon in zones 3-4 corresponds to the percentage of carbon in the deposited metal.

## ACKNOWLEDGMENTS

Investigation of the grain structures is performed according to the Government research assignment for ISPMS SB RAS, project FWRW-2021-0005.

## REFERENCES

- GOST R 57558-2017 Additive technological processes. Basic principles. Part 1. Terms and definitions.
- Murr, L.E., Martinez, E., Amato, K.N., et al. (2012), *Fabrication of metal and alloy components by additive manufacturing: examples of 3D materials science*, J Mater. Res. Technol. 1(1): 42-54. doi: 10.1016/S2238-7854(12)70009-1
- Murr, L.E., Gaytan, S.M., Ramirez, D.A., et al. (2012), *Metal fabrication by additive manufacturing using laser and electron beam melting technologies*, J Mater. Sci. Technol. 28:1: 1-14. doi: 10.1016/S1005-0302(12)60016-4
- Gu, D.D., Meiners, W., Wissenbach, K., Poprawe, R. (2012), *Laser additive manufacturing of metallic components: materials, processes and mechanisms*, Int. Mater. Rev. 57:3: 133-164. doi: 10.1179/1743280411Y.0000000014
- Sing, S.L., An, J., Yeong, W.Y., Wiria, F.E. (2016), *Laser and electron-beam powder-bed additive manufacturing of metallic implants: A review on processes, materials and designs*, J Orthop. Res. 34(3): 369-385. doi: 10.1002/jor.23075
- Körner, C. (2016), *Additive manufacturing of metallic components by selective electron beam melting - a review*, Int. Mater. Rev. 61(5): 361-377. doi: 10.1080/09506608.2016.1176289
- Herzog, D., Seyda, V., Wycisk, E., Emmelmann, C. (2016), *Additive manufacturing of metals*, Acta Materialia, 117: 371-392. doi: 10.1016/j.actamat.2016.07.019
- Harun, W.S.W., Manam, N.S., Kamariah, M.S.I.N., et al. (2018), *A review of powdered additive manufacturing techniques for Ti-6Al-4V biomedical applications*, Powder Technol. 331: 74-97. doi: 10.1016/j.powtec.2018.03.010
- Chen, S., Tong, Y., Liaw, P.K. (2018), *Additive manufacturing of high-entropy alloys: A review*, Entropy, 20(12): 937. doi: 10.3390/e20120937
- Ahmed, N. (2019), *Direct metal fabrication in rapid prototyping: A review*, J Manuf. Proc. 42: 167-191. doi: 10.1016/j.jmapro.2019.05.001
- Frazier, W.E. (2014), *Metal additive manufacturing: A review*, J Mater. Eng. Perf., 23: 1917-1928. doi: 10.1007/s11665-014-0958-z
- Sames, W.J., List, F.A., Pannala, S., et al. (2016), *The metallurgy and processing science of metal additive manufacturing*, Int. Mater. Rev. 61(5): 315-360. doi: 10.1080/09506608.2015.1116649
- Murr, L.E. (2018), *A Metallographic review of 3D printing/additive manufacturing of metal and alloy products and components*, Metal. Microstr. Anal. 7(2): 103-132. doi: 10.1007/s13632-018-0433-6

14. Kok, Y., Tan, X.P., Wang, P., et al. (2018), *Anisotropy and heterogeneity of microstructure and mechanical properties in metal additive manufacturing: A critical review*, Mater. Des. 139: 565-586. doi: 10.1016/j.matdes.2017.11.021
15. DebRoy, T., Wei, H.L., Zuback, J.S., et al. (2018), *Additive manufacturing of metallic components - Process, structure and properties*, Prog. Mater. Sci. 92: 112-224. doi: 10.1016/j.pmatsci.2017.10.001
16. Gisario, A., Kazarian, M., Martina, F., Mehrpouya, M. (2019), *Metal additive manufacturing in the commercial aviation industry: A review*, J Manuf. Syst. 53: 124-149. doi: 10.1016/j.jmsy.2019.08.005
17. Li, N., Huang, S., Zhang, G., et al. (2019), *Progress in additive manufacturing on new materials: A review*, J Mater. Sci. Technol. 35(2): 242-269. doi: 10.1016/j.jmst.2018.09.002
18. Ding, D., Pan, Z., Cuiuri, D., Li, H. (2015), *Wire-feed additive manufacturing of metal components: technologies, developments and future interests*, Int. J Adv. Manuf. Technol. 81: 465-481. doi: 10.1007/s00170-015-7077-3
19. Oliveira, J.P., Santos, T.G., Miranda, R.M. (2020), *Revisiting fundamental welding concepts to improve additive manufacturing: From theory to practice*, Prog. Mater. Sci. 107: 100590. doi: 10.1016/j.pmatsci.2019.100590
20. Williams, S.W., Martina, F., Addison, A.C., et al. (2016), *Wire + arc additive manufacturing*, Mater. Sci. Technol. 32(7): 641-647. doi: 10.1179/1743284715Y.0000000073
21. Wu, B., Pan, Z., Ding, D., et al. (2018), *A review of the wire arc additive manufacturing of metals: properties, defects and quality improvement*, J Manuf. Proc. 35: 127-139. doi: 10.1016/j.jmapro.2018.08.001
22. Cunningham, C.R., Flynn, J.M., Shokrani, A., et al. (2018), *Invited review article: Strategies and processes for high quality wire arc additive manufacturing*, Add. Manuf. 22: 672-686. doi: 10.1016/j.addma.2018.06.020
23. Brandl, E., Michailov, V., Viehweger, B., Leyens, C. (2011), *Deposition of Ti-6Al-4V using laser and wire, part I: Microstructural properties of single beads*, Surf. Coat. Technol. 206 (6): 1120-1129. doi: 10.1016/j.surfcoat.2011.07.095
24. Brandl, E., Michailov, V., Viehweger, B., Leyens, C. (2011), *Deposition of Ti-6Al-4V using laser and wire, part II: Hardness and dimensions of single beads*, Surf. Coat. Technol. 206 (6): 1130-1141. doi: 10.1016/j.surfcoat.2011.07.094
25. Brandl, E., Palm, F., Michailov, V., et al. (2011), *Mechanical properties of additive manufactured titanium (Ti-6Al-4V) blocks deposited by a solid-state laser and wire*, Mater. Des. 32(10): 4665-4675. doi: 10.1016/j.matdes.2011.06.062
26. Ding, Y., Akbari, M., Kovacevic, R. (2018), *Process planning for laser wire-feed metal additive manufacturing system*, Int. J Adv. Manuf. Technol. 95(1-4): 355-365. doi: 10.1007/s00170-017-1179-z
27. Chekir, N., Sixsmith, J.J., Tollett, R., Brochu, M. (2019), *Laser wire deposition of a large Ti-6Al-4V space component*, Weld. J 98(6): 172-s-180-s. doi: 10.29391/2019.98.014
28. Gibson, B.T., Bandari, Y.K., Richardson, B.S., et al. (2020), *Melt pool size control through multiple closed-loop modalities in laser-wire directed energy deposition of Ti-6Al-4V*, Add. Manuf. 32: 100993. doi: 10.1016/j.addma.2019.100993
29. Tarasov, S.Yu., Filippov, A.V., Savchenko, N.L., et al. (2018), *Effect of heat input on phase content, crystalline lattice parameter, and residual strain in wire-feed electron beam additive manufactured 304 stainless steel*, Int. J Adv. Manuf. Technol. 99: 2353-2363. doi: 10.1007/s00170-018-2643-0
30. Fuchs, J., Schneider, C., Enzinger, N. (2018), *Wire-based additive manufacturing using an electron beam as heat source*, Weld. World, 62(2): 267-275. doi: 10.1007/s40194-017-0537-7
31. Wanjara, P., Watanabe, K., de Formanoir, C., et al. (2019), *Titanium alloy repair with wire-feed electron beam additive manufacturing technology*, Adv. Mater. Sci. Eng. 2019: Art. ID 3979471. doi: 10.1155/2019/3979471
32. Martina, F., Mehnen, J., Williams, S.W., et al. (2012), *Investigation of the benefits of plasma deposition for the additive layer manufacture of Ti-6Al-4V*, J Mater. Proc. Technol. 212(6): 1377-1386. doi: 10.1016/j.jmatprotec.2012.02.002
33. Zhang, J., Wang, X., Paddea, S., Zhang, X. (2016), *Fatigue crack propagation behaviour in wire+arc additive manufactured Ti-6Al-4V: Effects of microstructure and residual stress*, Mater. Des. 90: 551-561. doi: 10.1016/j.matdes.2015.10.141
34. Lin, J., Lv, Y., Liu, Y., et al. (2017), *Microstructural evolution and mechanical property of Ti-6Al-4V wall deposited by continuous plasma arc additive manufacturing without post heat treatment*, J Mech. Behav. Biomed. Mater. 69: 19-29. doi: 10.1016/j.jmbbm.2016.12.015
35. Hönnige, J.R., Colegrove, P., Williams, S. (2017), *Improvement of microstructure and mechanical properties in wire + arc additively manufactured Ti-6Al-4V with machine hammer peening*, Proc. Eng. 216: 8-17. doi: 10.1016/j.proeng.2018.02.083
36. Lin, J., Lv, Y., Guo, D., et al. (2019), *Enhanced strength and ductility in thin Ti-6Al-4V alloy components by alternating the thermal cycle strategy during plasma arc additive manufacturing*, Mater. Sci. Eng.: A, 759: 288-297. doi: 10.1016/j.msea.2019.05.025
37. Ríos, S., Colegrove, P.A., Williams, S.W. (2019), *Metal transfer modes in plasma wire + arc additive manufacture*, J Mater. Proc. Tech. 264: 45-54. doi: 10.1016/j.jmatprotec.2018.08.043
38. Biswal, R., Zhang, X., Shamir, M., et al. (2019), *Interrupted fatigue testing with periodic tomography to monitor porosity defects in wire + arc additive manufactured Ti-6Al-4V*, Add. Manuf. 28: 517-527. doi: 10.1016/j.addma.2019.04.026
39. McAndrew, A.R., Rosales, M.A., Colegrove, P.A., et al. (2018), *Interpass rolling of Ti-6Al-4V wire+arc additively manufactured features for microstructural refinement*, Add. Manuf. 21: 340-349. doi: 10.1016/j.addma.2018.03.006
40. Martina, F., Roy, M.J., Szost, B.A., et al. (2016), *Residual stress of as-deposited and rolled wire+arc additive manufacturing Ti-6Al-4V components*, Mater. Sci. Technol. 32(14): 1439-1448. doi: 10.1080/02670836.2016.1142704
41. Donoghue, J., Antonysamy, A.A., Martina, F., et al. (2016), *The effectiveness of combining rolling deformation with wire-arc additive manufacture on  $\beta$ -grain refinement and texture modification in Ti-6Al-4V*, Mater. Charact. 114: 103-114. doi: 10.1016/j.matchar.2016.02.001
42. Wu, B., Pan, Z., Chen, G., et al. (2019), *Mitigation of thermal distortion in wire arc additively manufactured Ti6Al4V part using active interpass cooling*, Sci. Technol. Weld. Join. 24(5): 484-494. doi: 10.1080/13621718.2019.1580439
43. Lu, T., Liu, C., Li, Z., et al. (2020), *Hot-wire arc additive manufacturing Ti-6.5Al-2Zr-1Mo-1V titanium alloy: pore characterization, microstructural evolution, and mechanical properties*, J Alloys Comp. 817: 153334. doi: 10.1016/j.jallcom.2019.153334
44. Elmer, J.W., Gibbs, G. (2019), *The effect of atmosphere on the composition of wire arc additive manufactured metal components*, Sci. Technol. Weld. Join. 24(5): 367-374. doi: 10.1080/13621718.2019.1605473
45. Queguineur, A., Rückert, G., Cortial, F., Hascœt, J.Y. (2018), *Evaluation of wire arc additive manufacturing for large-sized components in naval applications*, Weld. World, 62(2): 259-266. doi: 10.1007/s40194-017-0536-8
46. Rodriguez, N., Vázquez, L., Huarte, I., et al. (2018), *Wire and arc additive manufacturing: a comparison between CMT and TopTIG processes applied to stainless steel*, Weld. World, 62: 1083-1096. doi: 10.1007/s40194-018-0606-6



47. Bekker, A.C.M., Verlinden, J.C. (2018), *Life cycle assessment of wire+arc additive manufacturing compared to green sand casting and CNC milling in stainless steel*, J Clean. Prod. 177: 438-447. doi: 10.1016/j.jclepro.2017.12.148
48. Hofer, K., Haelsig, A., Mayr, P. (2018), *Arc-based additive manufacturing of steel components - comparison of wire- and powder-based variants*, Weld. World, 62: 243-247. doi: 10.1007/s40194-017-0527-9
49. Martina, F., Ding, J., Williams, S., et al. (2019), *Tandem metal inert gas process for high productivity wire arc additive manufacturing in stainless steel*, Add. Manuf. 25: 545-550. doi: 10.1016/j.addma.2018.11.022
50. Hosseini, V.A., Höglström, M., Hurtig, K., et al. (2019), *Wire-arc additive manufacturing of a duplex stainless steel: thermal cycle analysis and microstructure characterization*, Weld. World, 63: 975-987. doi: 10.1007/s40194-019-00735-y
51. Ahsan, M.R.U., Tanvir, A.N.M., Seo, G.-J., et al. (2020), *Heat-treatment effects on a bimetallic additively-manufactured structure (BAMS) of the low-carbon steel and austenitic-stainless steel*, Add. Manuf. 32: 101036. doi: 10.1016/j.addma.2020.101036
52. Laghi, V., Palermo, M., Gasparini, G., et al. (2020), *Experimental results for structural design of wire-and-arc additive manufactured stainless steel members*, J Construct. Steel Res. 167: 105858. doi: 10.1016/j.jcsr.2019.105858
53. Elmer, J.W., Vaja, J., Carpenter, J.S., et al. (2020), *Wire-based additive manufacturing of stainless steel components*, Weld. J, 99: 8-s-24-s. doi: 10.29391/2020.99.002
54. Li, F., Chen, S., Shi, J., Zhao, Y. (2019), *In-process control of distortion in wire and arc additive manufacturing based on a flexible multipoint support fixture*, Sci. Technol. Weld. Join. 24 (1): 36-42. doi: 10.1080/13621718.2018.1476083
55. Gomez Ortega, A., Corona Galvan, L., Deschaux-Beaume, F., et al. (2018), *Effect of process parameters on the quality of aluminium alloy AlSi deposits in wire and arc additive manufacturing using a cold metal transfer process*, Sci. Technol. Weld. Join. 23(4): 316-332. doi: 10.1080/13621718.2017.1388995
56. Geng, H., Li, J., Xiong, J., Lin, X. (2017), *Optimisation of interpass temperature and heat input for wire and arc additive manufacturing 5A06 aluminium alloy*, Sci. Technol. Weld. Join. 22(6): 472-483. doi: 10.1080/13621718.2016.1259031
57. Gomez Ortega, A., Corona Galvan, L., Salem, M., et al. (2019), *Characterisation of 4043 aluminium alloy deposits obtained by wire and arc additive manufacturing using a cold metal transfer process*, Sci. Technol. Weld. Join. 24(6): 538-547. doi: 10.1080/13621718.2018.1564986
58. Zhang, S., Zhang, Y., Gao, M., et al. (2019), *Effects of milling thickness on wire deposition accuracy of hybrid additive/subtractive manufacturing*, Sci. Technol. Weld. Join. 24(5): 375-381. doi: 10.1080/13621718.2019.1595925
59. Gu, J., Yang, S., Gao, M., et al. (2020), *Micropore evolution in additively manufactured aluminum alloys under heat treatment and inter-layer rolling*, Mater. Des. 186: 108288. doi: 10.1016/j.matdes.2019.108288
60. Zhang, Z., Ren, W., Yang, Z., Wen, G. (2020), *Real-time seam defect identification for Al alloys in robotic arc welding using optical spectroscopy and integrating learning*, Measurement, 156: 107546. doi: 10.1016/j.measurement.2020.107546
61. Miao, Q., Wu, D., Chai, D., et al. (2020), *Comparative study of microstructure evaluation and mechanical properties of 4043 aluminum alloy fabricated by wire-based additive manufacturing*, Mater. Des. 186: 108205. doi: 10.1016/j.matdes.2019.108205
62. Javadi, Y., MacLeod, C.N., Pierce, S.G., et al. (2019), *Ultrasonic phased array inspection of a Wire + Arc Additive Manufactured (WAAM) sample with intentionally embedded defects*, Add. Manuf. 29: 100806. doi: 10.1016/j.addma.2019.100806
63. Horii, T., Kirihara, S., Miyamoto, Y. (2008), *Freeform fabrication of Ti-Al alloys by 3D micro-welding*, Intermetallics 16 (11-12): 1245-1249. doi: 10.1016/j.intermet.2008.07.009
64. Ou, W., Mukherjee, T., Knapp, G.L., et al. (2018), *Fusion zone geometries, cooling rates and solidification parameters during wire arc additive manufacturing*, Int. J Heat Mass Transf. 127: 1084-1094. doi: 10.1016/j.ijheatmasstransfer.2018.08.111
65. Marinelli, G., Martina, F., Ganguly, S., Williams, S. (2019), *Development of Wire + Arc additive manufacture for the production of large-scale unalloyed tungsten components*, Int. J Refract. Met. Hard Mater. 82: 329-335. doi: 10.1016/j.ijrmhm.2019.05.009
66. Marinelli, G., Martina, F., Lewtas, H., et al. (2019), *Microstructure and thermal properties of unalloyed tungsten deposited by wire + arc additive manufacture*, J Nucl. Mater. 522: 45-53. doi: 10.1016/j.jnucmat.2019.04.049
67. Abe, T., Mori, D., Sonoya, K., et al. (2019), *Control of the chemical composition distribution in deposited metal by wire and arc-based additive manufacturing*, Precis. Eng. 55: 231-239. doi: 10.1016/j.precisioneng.2018.09.010
68. Zeng, Z., Cong, B.Q., Oliveira, J.P., et al. (2020), *Wire and arc additive manufacturing of a Ni-rich NiTi shape memory alloy: Microstructure and mechanical properties*, Add. Manuf. 32: 101051. doi: 10.1016/j.addma.2020.101051
69. Kuznetsov, M.A., Danilov, V.I., Krampit, M.A., et al. (2020), *Mechanical and tribological properties of a metal wall grown by an electric arc method in an atmosphere of shielding gas*, Obrabotka Metallov - Metal Work. Mater. Sci. 22(3): 18-32. doi: 10.17212/1994-6309-2020-22.3-18-32
70. Kuznetsov, M.A., Zernin, E.A., Krampit, M.A., et al. (2019), *Structural and chemical analysis of 3D printed metal products*, Int. J Adv. Sci. Technol. 28(15): 699-709.
71. Saprykina, N.A., Proskokov, A.V., Saprykin, A.A. (2020), *Structural synthesis of mechanisms kinematics-type delta*, Fund. Appl. Probl. Eng. Technol. 2020(1) (339): 26-33. doi: 10.33979/2073-7408-2020-339-1-26-33
72. Saprykina, N.A., Proskokov, A.V., Saprykin, A.A. (2020), *Kinematic and dynamic analysis of a linear delta robot*, Handbook, An Eng. J, 2020(5): 27-32. doi: 10.14489/hb.2020.05.pp.027-032
73. Kuznetsov, M.A., Ilyashchenko, D.P., Verkhoturouva, E.V. (2022), *Manufacture of metal products by arc methods of melting welding wire*, Fund. Appl. Probl. Eng. Technol. 2022(2) (352): 41-52. doi: 10.33979/2073-7408-2022-352-2-41-51
74. Arzamasov, B.N., Makarova, V.I., Mukhin, G.G. et al.; B.N. Arzamasova, G.G. Mukhin (Eds.), *Materials Science: A Textbook for Universities*, 3<sup>rd</sup> Ed., Publishing House of MSTU im. N.E. Bauman, 2002. (in Russian)
75. Kakhovsky, N.I., Fartushny, V.G., Yushchenko, K.A., *Electric Arc Welding of Steels*, Handbook, Publishing House 'Naukova Dumka', Kiev, 1975. (in Russian)

© 2024 The Author. Structural Integrity and Life. Published by DIVK (The Society for Structural Integrity and Life 'Prof. Dr Stojan Sedmak') (<http://divk.inovacionicentar.rs/ivk/home.html>). This is an open access article distributed under the terms and conditions of the Creative Commons Attribution-NonCommercial-NoDerivatives 4.0 International License